



HAL
open science

A Comparative Study on the Nonlinear Interaction Between a Focusing Wave and Cylinder Using State-of-the-art Solvers: Part B

Shagun Agarwal, Shaswat Saincher, Sriram Venkatachalam, Shiqiang Yan,
Zihua Xie, Torsten Schlurmann, Qingwei Ma, Xiaotong Yang, Decheng Wan,
Jiaye Gong, et al.

► **To cite this version:**

Shagun Agarwal, Shaswat Saincher, Sriram Venkatachalam, Shiqiang Yan, Zihua Xie, et al.. A Comparative Study on the Nonlinear Interaction Between a Focusing Wave and Cylinder Using State-of-the-art Solvers: Part B. International Journal of Offshore and Polar Engineering (IJOPE), 2021, 31 (1), pp.11-18. 10.17736/ijope.2021.jc832 . hal-03261108

HAL Id: hal-03261108

<https://hal.science/hal-03261108>

Submitted on 28 Jun 2024

HAL is a multi-disciplinary open access archive for the deposit and dissemination of scientific research documents, whether they are published or not. The documents may come from teaching and research institutions in France or abroad, or from public or private research centers.

L'archive ouverte pluridisciplinaire **HAL**, est destinée au dépôt et à la diffusion de documents scientifiques de niveau recherche, publiés ou non, émanant des établissements d'enseignement et de recherche français ou étrangers, des laboratoires publics ou privés.



Distributed under a Creative Commons Attribution 4.0 International License

A Comparative Study on the Nonlinear Interaction Between a Focusing Wave and Cylinder Using State-of-the-art Solvers: Part B

Shagun Agarwal¹, Shaswat Saincher¹, V. Sriram¹, Shiqiang Yan^{*2}, Zhihua Xie^{*3}, Torsten Schlurmann⁴, Qingwei Ma^{*2}, Xiaotong Yang⁵, Decheng Wan^{*5}, Jiaye Gong^{*6}, Yunbo Li⁶, Yanyan Li^{*7}, Jinshu Lu^{*7}, Hanbing Sun⁸, Yan Liu⁹, Beilei Zou⁹, Shuling Chen⁹, Jing Lu¹⁰, Jianguo Lin¹⁰, Sa Young Hong^{*11}, Yoon-Jin Ha¹¹, Kyong-Hwan Kim^{*11}, Seok-Kyu Cho¹¹, Dong-Min Park¹¹, Aliyar Sithik^{1, 12}, Benjamin Bouscasse¹², Guillaume Ducrozet¹², Pierre Ferrant^{*12}

¹Indian Institute of Technology Madras, India; ²City, University of London, UK; ³Cardiff University, UK; ⁴Leibniz University of Hannover, Germany; ⁵Shanghai Jiao Tong University, China; ⁶Shanghai Maritime University, China; ⁷Zhejiang Ocean University, China; ⁸Harbin Engineering University, China; ⁹Jiangsu University of Science and Technology, China; ¹⁰Dalian Maritime University, China; ¹¹Korea Research Institute of Ships and Ocean Engineering, Korea; ¹²École Centrale Nantes, France

In this paper, the comparative study carried out for focused wave interaction with a moving cylinder in ISOPE-2020 is reported. The fixed cylinder cases are reported in the companion paper as Part A (Sriram, Agarwal, Yan et al., 2021). The paper discusses qualitative and quantitative comparison between four different numerical solvers that participated in this comparative study. This is a challenging problem, as the cylinder moves over 40 m and interacts with the focusing waves. The performance of various solvers is compared for two different moving cylinder speeds. Both weakly coupled models and full Navier–Stokes (NS) solvers with different strategies for modeling the cylinder motion were adopted by the participants. In particular, different methods available for numerically simulating the forward speed problem emerge from this paper. The qualitative comparison based on the wave probe and pressure probe time histories between laminar and turbulent solvers is presented. Furthermore, the quantitative error analysis for individual solvers shows deviations up to 30% for moving wave probes and 50% for pressure time history. The reliability of each method is discussed based on all the wave probe and pressure probe discrepancies against experiments. The deviations for higher speed shown by all solvers indicate that further improvements in the modeling capabilities are required.

INTRODUCTION

Nonlinear wave current–structure interaction is a topic of great interest for offshore and coastal engineering as well as naval architecture. However, the problem is challenging and complex due to the nonlinear wave–current process and its subsequent interactions with structure. Traditionally, due to the complication of generating constant current in the laboratory, researchers resort to towing the structure (Koterayama, 1984; Sarpkaya and Storm, 1985; Teng and Nath, 1985; Vengatesan et al., 2000; Shafieefar and Massie, 2001). Modeling extreme scenarios of nonlinear focused waves (or steep waves) superposed with a current of higher intensity can be achieved by this method as generation of focused waves over a current in an experimental facility is challenging (Stagonas et al., 2018). Towing introduces a local current near the structure that is sufficient to evaluate combined wave-current loads on the structure. Nevertheless, a depth-uniform current never exists in practice (Beyer et al., 2017; Chen et al., 2019), and it is only of academic and fundamental interests to understand the physics of nonlinear wave-current loading on a structure. Furthermore, a depth-uniform current would naturally impart more load than the depth-varying current, and hence the towing approach is conservative in nature. By towing the structure, nonlinear wave-current interactions are physically excluded, which facilitates simulating interactions between the combined field and a structure by the

numerical modeling community. However, numerical modeling is still challenging for larger towing speeds, where numerical stability and other complex physical processes in the wake region need to be modeled (Yan et al., 2015). This is particularly the case when a fixed reference frame-based simulation approach is adopted, which would require progressively larger domains with increasing towing speed.

The experimental measurements of the moving cylinder interacting with focused waves are released for the ISOPE-2020 participants. This paper discusses the performance of the recent numerical solvers for this complex problem of towing the structure with incoming waves. This benchmark case will be of particular interest to the forward speed problem in naval architecture, apart from studying the wave-current–cylinder interactions in other fields. In Part A (Sriram, Agarwal, Yan et al., 2021), we discussed the numerical performance based on 20 different solvers for wave–fixed-cylinder interactions. However, for a moving cylinder we had only four different solvers. The reason is the complexity of the problem; in particular, the cylinder needs to move over 40 m and then interact with the focusing waves. Herein, the focusing wave has to be fully developed whilst the cylinder should interact at the focusing locations with the same speed. Hence, the performance of the solvers or methodology adopted by the participants for this complex problem has been discussed, and the reliability of the approach in capturing: (a) the wave profile in the vicinity of the moving cylinder and propagation of waves in moving framework, and (b) the pressure time history at different probe locations above and below the still water level (SWL) for different towing speeds is analyzed. Finally, the methodology that provides the most robust solutions is identified and recommended for future studies.

*ISOPE Member.

Received January 9, 2021; revised manuscript received by the editors February 1, 2021. The original version was submitted directly to the Journal.

KEY WORDS: Comparative study, hybrid modeling, Navier–Stokes, potential flow theory, moving cylinder, validation.

Case	f_c (Hz)	$\Delta f/f_c$	f_1 (Hz)	t_f (s)	N	G_a	V_{cyl} (m/s)
Case 4	0.68	1.00	0.34	38.0	32	0.002	0.34
Case 5	0.68	1.00	0.34	38.0	32	0.002	0.78

Table 1 Tested wave packet characteristics (Sriram, Agarwal, and Schlurmann, 2021)

EXPERIMENTAL SETUP AND TESTING CONDITIONS

The details about the experimental setup are reported in the companion paper by Sriram, Agarwal, and Schlurmann (2021) and will not be repeated here for the sake of brevity. The tested wave characteristics reported in this paper are shown in Table 1.

From Table 1, one could see that same wave characteristics are provided, i.e., center frequency (f_c), bandwidth ratio (Δf), number of components (N), and wave steepness (via $G_a = 0.002$). However, two different towing speeds, $V_{cyl} = 0.34$ and 0.78 m/s, are considered for the cylinder. These correspond to currents of 1.86 m/s and 4.27 m/s, respectively, at the prototype scale, thus emulating extreme sea-state/storm conditions. Hence, the physical model test can be called a validation model.

PARTICIPATING CODES AND METHODOLOGY

In the present study, four different solvers have been used, and the details about the solvers are provided in Table 2. The solvers are broadly classified into two types: one that deals with one-way (or weakly) coupled fully nonlinear potential theory-Navier-Stokes (FNPT-NS) approach and the other with a full NS solver. In general, various possible approaches (MT1–MT4) to model the moving cylinder problem are shown in Fig. 1.

One may infer from Fig. 1 that, in the context of hybrid modeling, the two approaches MT1 and MT2 emerge based upon whether two-way or one-way coupling is considered between FNPT and NS. For the present study, one-way coupling is sufficient, and the authors employed this approach with one-way coupling. In MT1, the momentum equation is changed by adding a source term to simulate the effect of a towing-induced local current. However, in MT2, the entire domain along with the structure is moved. MT2 is numerically challenging to implement in comparison to MT1. Nevertheless, foamStar and qaleFOAM have adopted the MT2 approach. In the case of full NS solver, one can model it exactly as in experiments by moving the cylinder (MT3); however, complex dynamic meshing is required. The other option is moving the domain along with the structure using the overset

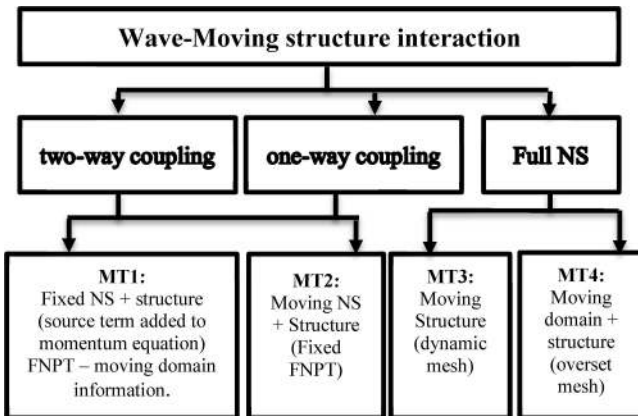


Fig. 1 Approaches to model wave-moving cylinder interactions

grid method (MT4). In terms of fidelity, the MT4 approach also closely emulates the actual experimental conditions. In the present case, participants using full NS chose the overset grid approach (MT4) rather than opting for computationally expensive dynamic meshing. The details about the capabilities of the various solvers may be referred to in the references listed in Table 2. It is worth noting that the qaleFOAM submissions showcase both laminar as well as turbulence modeling approaches to facilitate a comparison between both simulation strategies. STAR-CCM-KRISO used the Dirichlet method to generate waves instead of the piston-type wavemaker used in the experiments and preferred by other participants. All the solvers are based on two-phase flow using different interface capturing schemes.

RESULTS AND DISCUSSION

Performance of the Codes near the Wavemaker in Fixed Reference Frame (WP1)

The ability of the different participating codes to accurately generate the input wave packets, which would undergo focusing near the moving cylinder, is evaluated. To this effect, the free-surface elevation ($\eta(t)$) signals and wave spectra (only generated for studies that provided sufficiently long signals) measured by the fixed probe WP1 close to the wavemaker are compared for all the codes, as shown in Fig. 2. It is worth noting that the input (constant steepness) spectrum is the same across cases 4 and 5 (cf. Table 1). This is qualitatively evidenced from Figs. 2a and 2b and quantified by the spectra for case 5 (cf. Fig. 2c). However, it may be noticed that the same input signal appears time-shifted with the case 4 “peak” occurring ~ 7 s later (cf. Fig. 2a) than the case 5 peak (cf. Fig. 2b). This is attributed to the fact that the cylinder is towed at a slower speed for case 4 ($V_{cyl} = 0.34$ m/s) as compared to case 5 ($V_{cyl} = 0.78$ m/s), and the paddle input is accordingly delayed for case 4 to ensure that the wave packets correctly focus just before the moving cylinder in both cases. Broadly speaking, all participating codes were seen to generate the input wave packets with sufficient accuracy in both cases. Whilst this is true for the steepest wave of the group where the deviation in packet height is found to be $\gtrsim 2\%$, a larger deviation is observed for the packets that are generated after the steepest wave. For instance, the code naoFOAM-SJTU underpredicts the succeeding packet heights by $\sim 40\%$ for case 5 (see $t \sim 40$ s in Fig. 2b and $f \in [0.8, 1$ Hz] in Fig. 2c).

It is worth mentioning that even if this later mismatch were to be deemed unimportant in favor of the steepest wave, the said deviations may noticeably grow at the point of interaction, which is ~ 20 m downstream of WP1. Although 4 out of 5 studies adopt the piston wavemaker input either directly or through weak coupling, the Dirichlet input strategy (STAR-CCM-KRISO) is also observed to work perfectly fine.

Performance of the Codes for Wave-focusing and Wave-Wake Interactions in Moving Reference Frame (WP5–WP7)

Next, the participating codes are evaluated based on their ability to capture wave focusing as well as wave-wake interactions. As the free-surface elevation variations ($\eta(t)$) near the cylinder are recorded by probes mounted on the towing carriage (WP5–WP7), an additional challenge arises in that the validation is to be carried out in a reference frame moving at the cylinder speed. The $\eta(t)$ signals and wave spectra recorded by the moving wave probes are superimposed and compared for all the codes in Fig. 3.

S/N	Name of the participating university	Code name/label	P/NSL/ NST	Method	Approach in modeling	Wave generation	Test case submitted	N_{cells} (million)	L_{NS}	IH, IH, OS, C
1.	City, University of London Li et al. (2018); Yan et al. (2020)	qaleFOAM-H-City	P-NSL	FEM-FVM	MT2	Piston in P - WC	Case 4&5	6.27	4.0 m	IH/OS
2.	Shanghai Maritime University Li et al. (2018); Yan et al. (2020)	qaleFOAM-H-SMU	P-NSL k- ω SST	FEM-FVM	MT2	Piston in P- WC	Case 5	1.73	4.4 m	IH/OS
3.	Korea Research Institute of Ships and Ocean Engineering Ha et al. (2019)	STAR-CCM-KRISO	NSL	FVM	MT4	Dirichlet BCs	Case 4&5	\sim 0.80	NA	C
4.	Shanghai Jiao Tong University Shen and Wan (2016)	naoeFOAM-SJTU	NSL	FVM	MT4	Piston	Case 4&5	8.98	NA	IH/OS
5.	École Centrale Nantes/Indian Institute of Technology Madras Choi et al. (2020)	foamStar-ECN	P-NSL	HOS-FVM	MT2	Piston in HOS-NWT WC Grid2Grid	Case 4&5	2.68	1.25 m	IH/OS

(P: potential; NSL: NS-Laminar; NST: NS-Turbulent; IH: in-house; OS: open source; C: commercial; WC: weak coupling; L_{NS} : length of Navier–Stokes subdomain before cylinder in case of weak coupling; N_{cells} : total number of cells)

Table 2 Details about the participating institutes and numerical codes employed for simulation

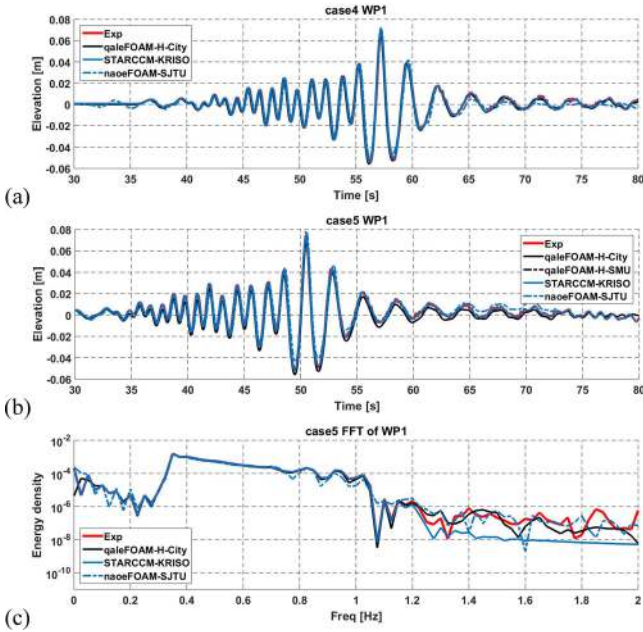


Fig. 2 Comparison of time series and wave spectra for surface elevation $\eta(t)$ recorded by the fixed probe WP1 near the wave paddle ($x = +4.98$ m) for (a) case 4 and (b, c) case 5

Here, it is worth noting that: (a) the performance of wave focusing is assessed at WP5–WP6, whilst (b) the accuracy of capturing interactions between focused waves and the cylinder wake is assessed at WP7.

It is observed from Fig. 3 that, for a given wave probe location, the level of agreement between individual studies deteriorates as V_{cyl} increases. In addition, for a fixed value of V_{cyl} , the level of

agreement between individual studies as well as against experiments is poor at WP5 (cf. Fig. 3a), decent at WP6 (cf. Fig. 3d), and very poor for WP7 (cf. Fig. 3g); this is especially true for case 5 with the larger towing speed. This behavior is linked to the hydrodynamics of the wave–moving cylinder interaction and can be explained by visualizing the passage of the focused wave crest past the towed structure; the same is depicted in Fig. 4 as a series of snapshots from foamStar-ECN simulations of case 5. The incident focused crest would first encounter WP5 in front of the cylinder. Here, the $\eta(t)$ signal recorded by WP5 would be a superposition of the incident wave elevation and the reflected “bulge of water formed” in front of the cylinder due to towing (cf. Fig. 4). This bulge would steepen with increasing V_{cyl} to the extent that it acts to “set up” the entirety of the $\eta(t)$ signal recorded by WP5. The fact that a couple of solvers indeed capture this setup proves that the same is attributable to the water bulging in front of the cylinder and not at the physical wave probe. This aspect of the problem is particularly tricky to validate at higher towing speeds, which explains the large scatter in $\eta(t)$ signals as well as spectra (cf. $f \in [0.4, 1$ Hz] in Fig. 3b) recorded at WP5 for case 5.

Referring to Fig. 4, WP6 is in-line with the cylinder center and almost in-line with the separation point, given that the Reynolds number based on the cylinder diameter is $\text{Re}_{\text{cyl}} \in [5.5 \times 10^4, 1.65 \times 10^5]$ for the problem at hand. However, given a lateral separation of $y = 71.5$ cm between WP6 and the surface of the cylinder (see Sriram, Agarwal, and Schlurmann, 2021), boundary layer separation is not expected to influence the free-surface topology at WP6. Furthermore, if one refers to the long-time $\eta(t)$ signals recorded by WP6 for cases 4 and 5 in the companion paper (Sriram, Agarwal, and Schlurmann, 2021), it can be noticed that the water bulge-induced setup is not as prominent at WP6 compared to WP5. Thus, there is an overall reduction in topological complexity at WP6 that is reflected in an improvement in agreement for $\eta(t)$ signals (cf. Figs. 3c and 3d). However, as men-

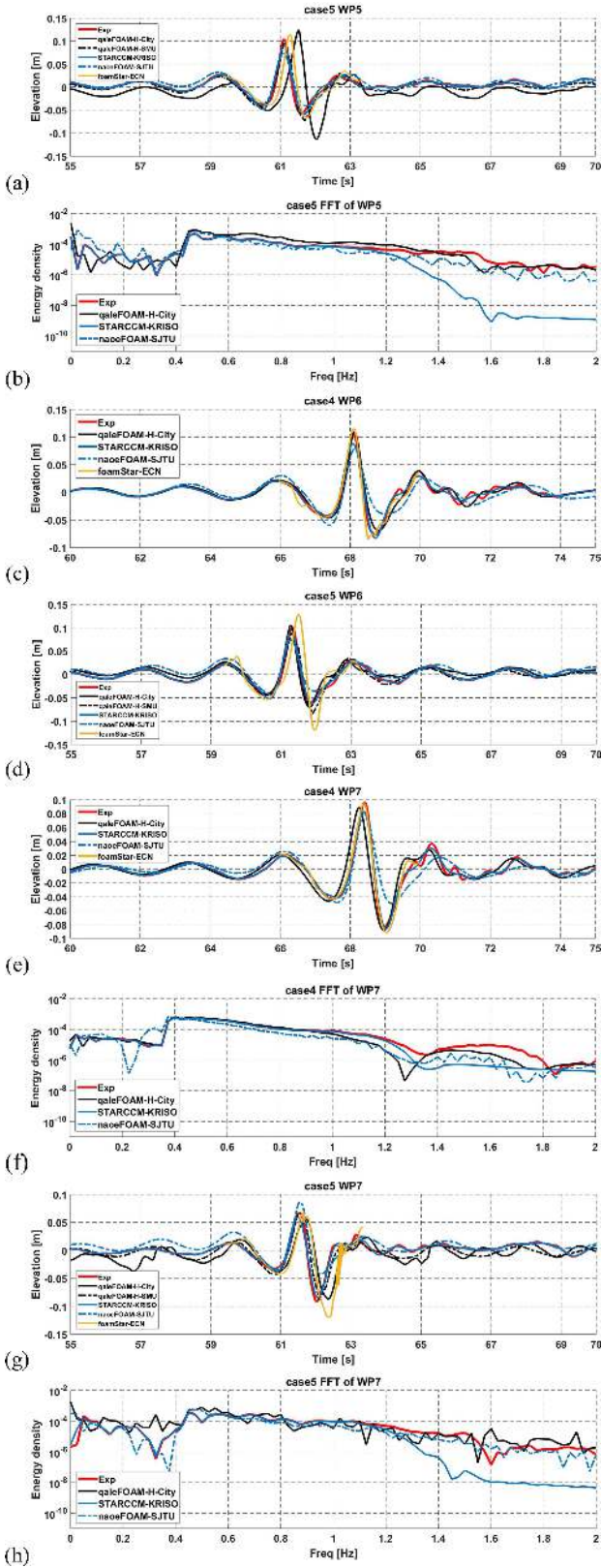


Fig. 3 Comparison of time series of $\eta(t)$ and wave spectra recorded by the moving probes WP5 ($x = -0.57$ m), WP6 ($x = 0$ m), and WP7 ($x = +0.71$ m); positions are with respect to the cylinder center.

tioned previously for WP7 within the wake region, the agreement between individual studies severely deteriorates. As evidenced from Figs. 3 and 4, pervasive short-wave generation occurs after

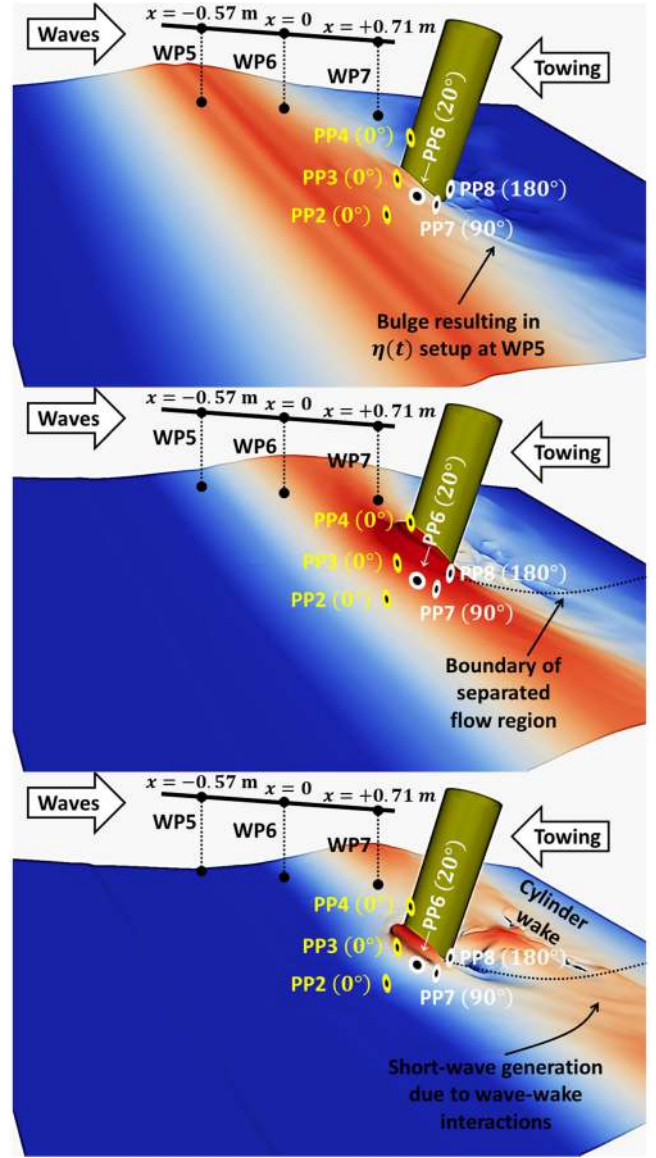


Fig. 4 Numerical snapshots of the moving cylinder interacting with the incident wave crest based on foamStar-ECN simulations of case 5. Positioning of the wave probes (WP) is relative to center of the cylinder. The reader is referred to the section on dynamic pressure for vertical (z) positioning of the pressure probes (PP).

passage of the main crest owing to wave–wake interactions; this is particularly the case at high towing speed (case 5). This is evidenced from a gain in spectral energy for $f > 1.2$ Hz at WP7 for case 5 (cf. Fig. 3h) when compared against the wave spectra generated at WP7 for case 4 (cf. Fig. 3f). This energy gain at higher frequency is also partly attributable to a general increase in the apparent frequency of the incoming waves for the higher towing speed. More importantly, at higher towing speed, the wave–wake interactions result in an overall reduction in wave height (due to viscous damping) with the trough elevation becoming greater than the crest elevation.

Thus, the validation exercise at WP7 demands that the solvers correctly capture the wake-induced viscous effects in addition to the short-wave generation following the main trough. This is challenging to say the least, as it requires a consistently refined streamwise mesh up to some distance downstream into the cylinder wake to capture the said phenomena. Thus, the large scatter

between various studies is to be expected in this case. Finally, an important observation emerging from the $\eta(t)$ records at WP7 for case 5 is that k - ω SST-based turbulence modeling (qaleFOAM-H-SMU) is outperformed by the commercial solver STAR-CCM-KRISO (abbreviated as SCK from this point forward) simulated using a laminar model. This indicates that, apart from turbulence modeling, mesh design and the accuracy of input wave packets generation are equally important parameters governing the success of a simulation. For instance, the aforementioned underprediction of input wave packet heights at WP1 by naoeFOAM-SJTU for case 5 (cf. Figs. 2b and 2c) results in a notable mismatch downstream at WP5–WP7 (cf. Figs. 3a, 3d, and 3g) and $f \in [0.6 : 1 \text{ Hz}]$ in Figs. 3b and 3h).

Accuracy in Capturing Dynamic Pressure During Wave-Current-Cylinder Interaction In Moving Reference Frame

Next, the ability of the various solvers to capture the dynamic pressure induced on the surface of the cylinder is analyzed; the hydrostatic contribution ($p = -\rho gz$) has been removed from the signal. As the moving cylinder is subjected to focused wave attack, the dynamic pressure is a combination of that induced by waves as well as the towing-induced current, locally acting on the structure. The dynamic pressure $p(t)$ signals recorded by the probes PP2, PP4, PP7, and PP8 have been superimposed for all the studies and reported in Fig. 5.

Broadly speaking, the agreement between the simulations and experiments in terms of the dynamic pressure shows similar trends as previously observed for the free-surface elevation signals. The extent of disagreement between the simulations and experiments, as well as between individual simulations, increases as V_{cyl} increases. Barring naoeFOAM-SJTU, where the underprediction in surface elevation is yet again reflected in the dynamic pressure values, the other solvers replicate the $p(t)$ history with notable accuracy at low towing speed (cf. Figs. 5a, 5c, 5e, and 5g). However, as the complexity of phenomena characterizing wave-moving cylinder interaction increases at higher towing speed (case 5), there is an equivalent reduction in the accuracy/fidelity of the simulations; this is clearly evidenced from Figs. 5b, 5d, 5f, and 5h). In case of PP2 (cf. Figs. 5a and 5b), the probe lies below the SWL ($z = -0.185 \text{ m}$) and is oriented at 0° facing wave attack. Thus, the trend of $p(t)$ variation closely resembles the $\eta(t)$ variations of the incident wave recorded at WP5 (cf. Figs. 3a and 3c). However, the towing-induced current loading acts to uniformly “set up” the $p(t)$ signal such that the “zero-crossings” in the signal no longer occur at atmospheric pressure but at the locally acting current pressure. This effect is naturally more prominent for case 5 (cf. Fig. 5b). It is worth noting that the supposed branching-off of the $p(t)$ signal at PP2 (and PP7) for case 5 at $t \sim 67 \text{ s}$ is due to differences in the point in time when the cylinder decelerated between different solvers. In particular, the PP2 and PP7 signals for qaleFOAM-H-SMU and naoeFOAM-SJTU indicate that the cylinder was kept in motion a little longer in comparison to the experiments. Hence, the $p(t)$ signal shows a tendency to rapidly move towards $p = 0$ in studies where the deceleration was triggered in accordance with the experiments. However, the probes continued to sense the current pressure for qaleFOAM-H-SMU and naoeFOAM-SJTU where the deceleration was probably triggered sometime later (cf. Fig. 5f). It can be observed that capturing the intermittent loading at PP4 (located at $z = +0.015 \text{ m}$ facing wave attack), as well as the boundary layer separation effects at PP7 (located below the SWL at $z = -0.085 \text{ m}$ and oriented at 90°), have proven to be especially challenging at high towing speed (cf. Figs. 5d and 5f). In

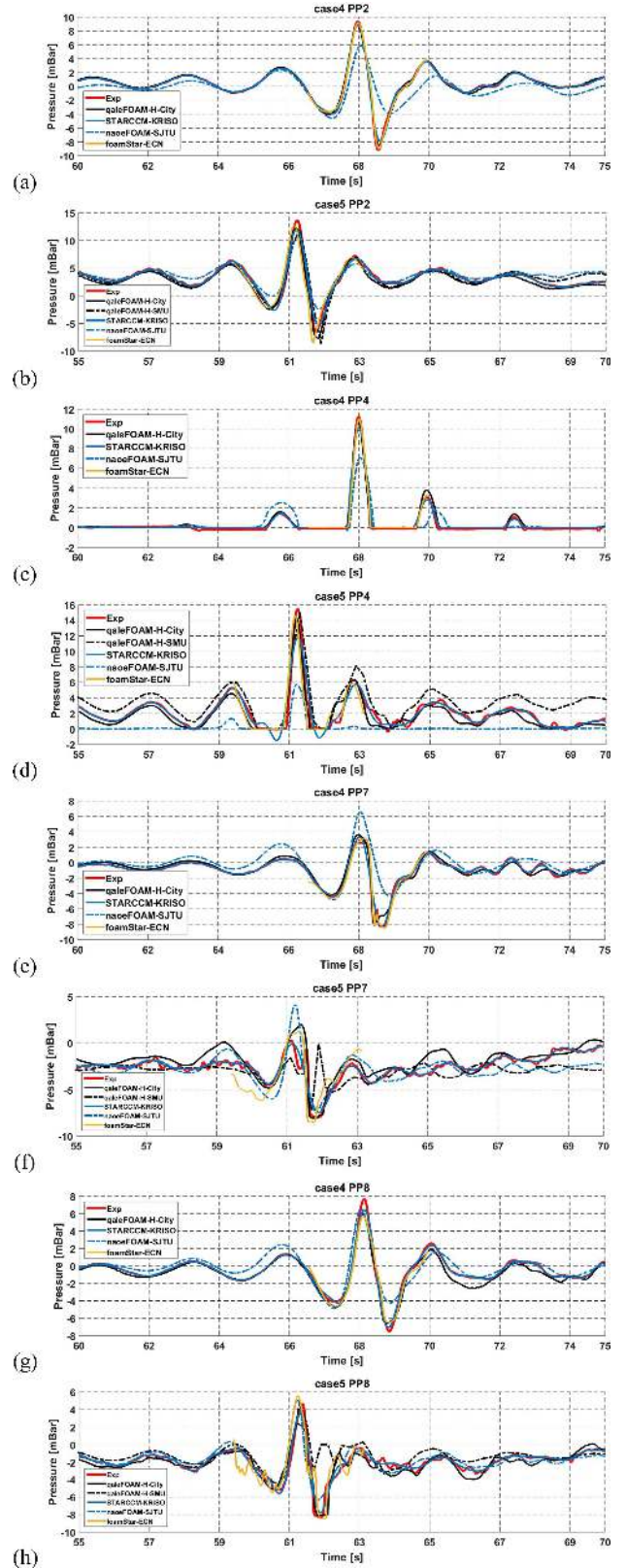


Fig. 5 Comparison of time series of dynamic pressure $p(t)$ signals recorded by the probes (a, b) PP2, (c, d) PP4, (e, f) PP7, and (g, h) PP8 mounted on the moving cylinder

this context the commercial solver SCK is observed to outperform the other participating codes. However, none of the solvers were able to capture the high-frequency oscillations triggered by wave-boundary layer and wave-wake interactions, respectively occur-

ring at PP7 (cf. Fig. 5f) and PP8 (cf. Fig. 5h), although the overall trend is indeed correctly captured by STAR-CCM-KRISO. It is also worth noting that the magnitude of suction is greater at the separation point (PP7), owing to a “nozzle-effect,” and the pressure deficit would be gradually recovered towards the rear-stagnation point (PP8) within the wake due to an antagonistic “diffuser-effect.” In fact, the towing-induced suction is so great at PP7 for case 5 that the passage of the focused crest barely restores hydrostatic conditions before the dynamic pressure again drops to -8 mBar at the following trough (cf. Fig. 5f). Considering qaleFOAM-H-SMU simulations, one may conclude from the pressure assessment that inclusion of turbulence modeling may not guarantee accurate capturing of boundary layer separation or wave–wake interactions (especially for the higher towing speed), and rather few of the laminar models exhibit better performance.

Quantification of Relative Errors

Thus far, the appraisal of participating codes towards capturing wave-moving cylinder interactions has been qualitative in nature; the same is now quantified in the present section. In the first stage of quantitative evaluation, the relative peak error in free-surface elevation ($(\eta_{\max}^{\text{num}} - \eta_{\max}^{\text{exp}})/\eta_{\max}^{\text{exp}}$) and pressure ($(p_{\max}^{\text{num}} - p_{\max}^{\text{exp}})/p_{\max}^{\text{exp}}$) has been plotted against the relative phase error in the respective peak values.

This is done for WP5–WP7, PP2–PP4, and PP6–PP8; the same is reported in Fig. 6. It should be noted that the outlier error values lying outside the shown range have not been plotted. Broadly speaking, the magnitude of relative peak error increases as V_{cyl} increases, whilst for a given towing speed, the relative error in peak pressure is considerably greater than that in the peak surface elevation. This is to be expected since the complex phenomena such as boundary layer separation, wave–wake interaction, and the resulting short-wave generation would be strongly manifested at the pressure probes mounted on the surface of the cylinder whilst the same would only be weakly manifested at the wave probes, which are laterally separated by ~ 70 cm from the cylinder surface

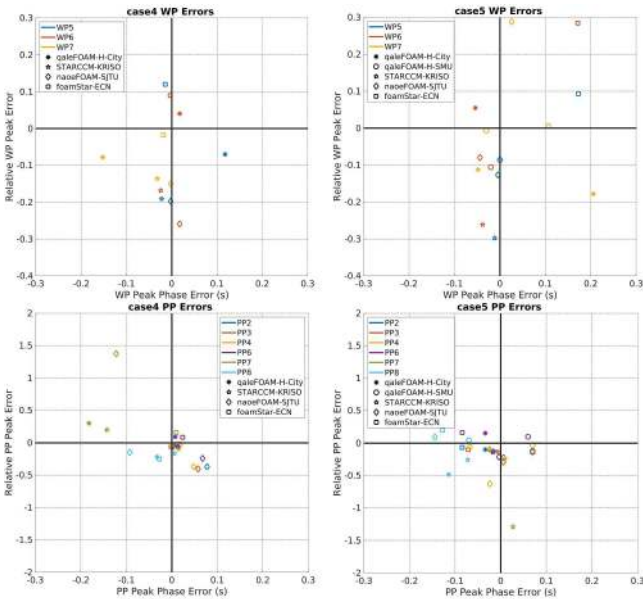


Fig. 6 Relative peak value error vs. peak phase error (s) for $\eta(t)$ and $p(t)$ signals recorded by the moving wave (WP5–WP7) and pressure (PP2–PP4 and PP6–PP8) probes for all participating codes

(cf. Sriram, Agarwal, and Schlurmann, 2021). Referring to the WP errors in Fig. 6, the only solvers that retain η_{\max} accuracy within $\pm 10\%$ error band for all three wave probes are qaleFOAM-H-City and qaleFOAM-H-SMU for cases 4 and 5, respectively. It should also be noted that, despite wave–wake interactions, the overall scatter in η_{\max} relative error is the least at WP7 for both cases 4 and 5.

Thus, although the participating codes disagree in terms of reproducing the $\eta(t)$ signal at WP7 (especially for case 5; cf. Fig. 3g), they show good agreement in replicating the peak surface elevation within the wake region. It is also worth noting that if one argues strictly in terms of the magnitude of the overall scatter in relative peak elevation error across WP5–WP7 for both towing speeds, SCK is seen to encounter the least scatter ($> 20\%$) amongst all the participating codes.

As mentioned previously in context of Fig. 6, the relative peak error values for pressure are considerably greater than those in free-surface elevation. The error spread in pressure is roughly $2\times$ larger than that in free-surface elevation for both towing speeds. Evidently, the greatest scatter occurs in PP7 for both cases 4 and 5 (cf. Figs. 5e and 5f). The abnormally large value of relative peak error observed for case 5 at PP7 (extreme outliers not shown) is attributable to the fact that, owing to strong suction induced at the separation point, the experimental PP7 peak itself is merely $p \sim 30$ Pa ($\sim 15\times$ smaller than the experimental PP8 peak), which is very close to the local hydrostatic pressure. This, coupled with the greater disagreement in $\eta(t)$ signals for case 5 (cf. Figs. 3a, 3d, and 3g), means that even a small deviation in replicating the experimental free-surface elevation at WP5 in the simulation would result in a large relative peak error at the separation point (PP7). This reasoning is corroborated by the fact that the error scatter at PP6 (20°) and PP8 (180°) is much smaller in

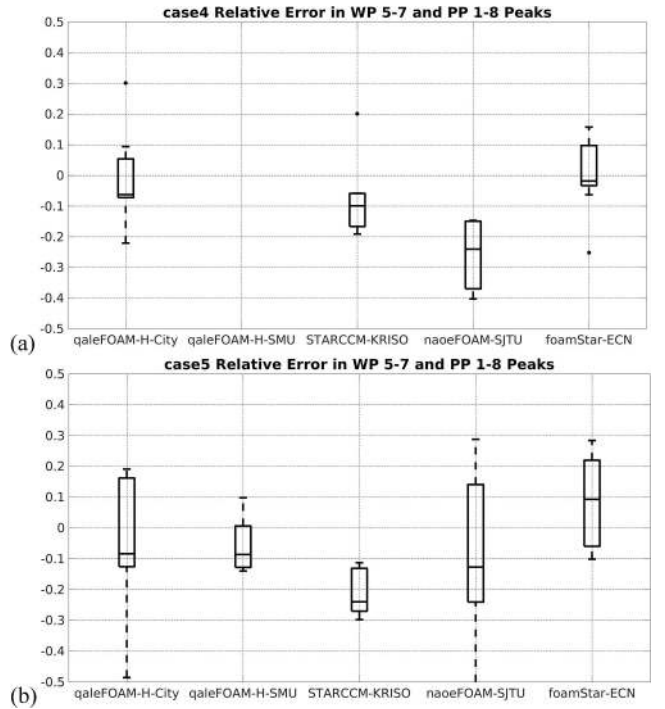


Fig. 7 Quartile-based representation of the relative error in peak values of surface elevation and pressure for (a) case 4 and (b) case 5 recorded at different probe locations and compared for all participating methods; qaleFOAM-H-SMU: only case 5 data submitted.

Sr.	Code name	Processor model	OpenMP, MPI, GPU, Serial	Number of CPUs (N_p)	Processor clock-speed (GHz)	System memory (RAM in GB)	Execution time for case 5 (T_{CPU})	Simulated time (T_{SIM})	$\frac{T_{CPU} \cdot N_p}{T_{SIM}}$ (case 5)
1.	qaleFOAM-H-City	Intel® Xeon® CPU E5-2680 v4	OpenMP MPI	16	2.4	64	71.11 hr	80 s	14.22 (hr for 1 s of simulation)
2.	qaleFOAM-H-SMU	Intel® Xeon® E5 2690 v3	MPI	7	2.4	32	–	19.5s	–
3.	STAR-CCM-KRISO	Intel® Xeon® CPU E5-2640 v4	MPI	300	2.4	192	~6 hr	80 s	22.5 (hr for 1 s of simulation)
4.	naoeFOAM-SJTU	Intel® Xeon® CPU E5-2680v3	MPI	39	2.6	64	184.2 hr	30 s	239.46 (hr for 1 s of simulation)
5.	foamStar-ECN	Intel® Xeon® CPU E5-2680v3 (Haswell-EP)	MPI	80	2.5	128	22.38 hr	60 s	29.84 (hr for 1 s of simulation)

Table 3 Computational aspects of the different solvers

comparison to that observed at PP7 (90°). Comparing the relative peak error values in PP (cf. Fig. 6) across individual solvers for case 4, it is observed that, barring an ~100% error scatter for naoeFOAM-SJTU, the magnitude of scatter is broadly comparable for the other codes; nonetheless, SCK shows the lowest scatter of ~37%.

When a similar comparison is made for case 5, SCK again exhibits the least overall scatter of ~115%. Here, one should be mindful of the fact that, for case 5, the difficulty in capturing the PP7 peak is responsible for the large error scatter observed across all studies (cf. Fig. 6). Thus, the comparatively lower scatter in the case of SCK is directly attributable to the closeness with which the solver was able to capture the PP7 peak (cf. Figs. 5e and 5f). Likewise, if the comparison were made without considering the PP7 errors, the minimum overall scatter for SCK drops to ~14%, which is very impressive. Finally, it may be noted that the majority of the solvers tend to overpredict the phase of the surface elevation peak by ~0.2 s, which is later reflected as a phase-shift in the pressure peak. However, the phase-shift is not considered a shortcoming from the standpoint of industrial applications where the magnitude of peak loads is of interest; the solvers’ performance is not judged based on this parameter. The individual solvers’ reliability in capturing the hydrodynamics of wave-moving cylinder interactions has eventually been summarized in the form of error quartiles in Fig. 7; each box plot is comprised of relative peak errors in $\eta(t)$ and $p(t)$ from all three wave and eight pressure probes, respectively.

In a broad sense, for a given code, the quartiles spread wider for the pressure measurements; this is to be expected in light of the preceding discussions. For case 4, the error spread is minimal for SCK, followed by foamStar-ECN (cf. Fig. 7a). For case 5, the error spread is again minimal for SCK, followed by the P-NST code qaleFOAM-H-SMU (cf. Fig. 7b). However, since results from the latter solver were only submitted for case 5, it is concluded that the commercial solver SCK with laminar model gives the best performance in terms of minimizing the overall error spread across both cases 4 and 5. This is strongly attributed to the accuracy with which the initial wave packets were generated (cf. Fig. 2a). Despite the small error spread, the box-plots indicate a tendency for SCK to underpredict $\eta(t)$ and $p(t)$ peak values, as the median error is approximately –15% in this case. Hence,

upon comparing the solvers on the basis of their ability to minimize the median relative peak error, it is seen that qaleFOAM-H-City gives the best performance with a median relative peak error in the range: [–10% : –6%]. With this, the quantitative reliability of the different solvers in capturing the hydrodynamics of wave-moving cylinder interactions is analyzed. The computational aspects of the different solvers are compared in the next and concluding section of this paper.

Comparison of CPU Effort

Given the fact that only four solvers participated in Part B of the comparative study involving a moving cylinder, only a limited amount of data could be collected toward comparing the CPU effort across different codes. Nevertheless, the same is reported for the sake of completeness in Table 3. Based on the number of CPUs employed (N_p), both SCK and foamStar-ECN can be said to have employed supercomputers for simulation, whilst the other three studies were executed on workstations. Considering the wide variation in the number of CPUs (N_p) and physical times (T_{SIM}) chosen by the participants, the overall “wall clock” or execution time (T_{CPU}) is seen to vary considerably across different studies. In an attempt to compare the solvers on a similar footing, we define the CPU effort as (Ransley et al., 2019): $(T_{CPU} \cdot N_p)/T_{SIM}$; the same is reported in Table 3 for simulations involving the higher towing speed. It can be seen that, for the same $T_{SIM} = 80$ s, the CPU effort is lower for the hybrid model qaleFOAM-H-City in comparison to the commercial NS solver SCK.

Thus, although employing a supercomputer definitely reduces computational time, it may not reduce CPU effort or improve computational efficiency. Instead, hybrid modeling of potential and viscous solvers goes a long way to improve the computational efficiency for large-scale simulations. The large CPU effort for naoeFOAM-SJTU is attributed to very high T_{CPU} , which is in turn attributable to the fact that this is a full-NS solver employing a ~9 million cell mesh for simulation.

CONCLUSIONS

The present paper reports on a comparative computational study of four state-of-the-art numerical solvers applied to the problem of nonbreaking focused waves interacting with a moving cylinder. The following observations are drawn from the investigation:

1. Wave packets, especially small-steepness waves close to the wavemaker, should be generated as accurately as possible, since small discrepancies may noticeably grow at the point of focusing, thus affecting pressures on the structure. This was shown from the different code performances.

2. In the context of capturing free-surface variations around the moving cylinder, the solvers are observed to achieve good agreement against experiments for low towing speed. At high towing speed, additional complications, such as bulging of water in front of the cylinder and strong 3D deformations of the waves in the cylinder wake, arise. These phenomena proved to be challenging to capture for 80% of the studies.

3. Validating the dynamic pressure at the separation (PP7) and rear stagnation points (PP8) at high towing speed proved to be particularly challenging, even for turbulence-based RANS model. The strong suction induced in the separation region at large towing speed can make the separation point pressure peak $\sim 15\times$ smaller than the peak pressure at the rear stagnation point. This resulted in a $2\times$ greater error spread for pressure in comparison to that in the free-surface elevation. Only one commercial code-based laminar model could capture the separation peak pressure with reasonable accuracy.

4. Taking all probe locations into consideration, the minimum overall scatter in relative error for free-surface elevation and pressure is $\sim 25\%$ for SCK and qaleFOAM-H-SMU. However, it is to be noted that the latter solver was only applied to the case with high towing speed whilst the former was applied to both towing speeds. The scatter in relative error is $\sim 50\%$ for the other solvers.

5. A new analysis procedure to check the reliability of the individual solvers (including all parameters) performance is provided. This can be used for future comparative studies.

The above observations may be taken into account whilst developing new or applying existing numerical algorithms toward simulating the interaction of focused waves with a moving structure in a large domain. Based on Part A (Sriram, Agarwal, Yan et al., 2021) and the present Part B paper, it was shown that the present modeling capability has been improved. In future comparative studies, apart from comparing with experiments, the intercomparisons of the codes for vorticity field, as well as turbulence field, can be attempted based on this success; however, experimental results may not be available. This should be the future direction of collaborative comparative studies in ISOPE.

ACKNOWLEDGEMENTS

The first author would like to acknowledge the PMRF fellowship. The second author would like to acknowledge support from the Institute Post-Doctoral fellowship of IIT Madras. The third author would like to thank the Alexander Von Humboldt Foundations and German Academic Exchange Service (DAAD), as well as DST-UKIERI project (2016-17-0029) for the experiments and numerical model developments in qaleFOAM between IITM and City, University of London, UK.

REFERENCES

Beyer, M, Swan, C, and Christou, M (2017). "Focused Waves on Depth-varying Currents: The Role of Vorticity," *Proc 27th Int Ocean Polar Eng Conf*, San Francisco, CA, USA, ISOPE, 1, 340–347.

Chen, LF, et al. (2019). "Numerical Modelling of Interactions of Waves and Sheared Currents with a Surface Piercing Vertical

Cylinder," *Coastal Eng*, 145, 65–83.
<https://doi.org/10.1016/j.coastaleng.2019.01.001>.

Choi, Y-M, et al. (2020). "Performance of Different Techniques of Generation and Absorption of Free-surface Waves in Computational Fluid Dynamics," *Ocean Eng*, 214, 107575.
<https://doi.org/10.1016/j.oceaneng.2020.107575>.

Ha, YJ, Nam, BW, Kim, KH, and Hong, SY (2019). "CFD Simulations of Wave Impact Loads on a Truncated Circular Cylinder by Breaking Waves," *Int J Offshore Polar Eng*, ISOPE, 29(3), 306–314. <https://doi.org/10.17736/ijope.2019.ak33>.

Koterayama, W (1984). "Wave Forces Acting on a Vertical Circular Cylinder with a Constant Forward Velocity," *Ocean Eng*, 11(4), 363–379. [https://doi.org/10.1016/0029-8018\(84\)90011-8](https://doi.org/10.1016/0029-8018(84)90011-8).

Li, Q, Wang, J, Yan, S, Gong, J, and Ma, QW (2018). "A Zonal Hybrid Approach Coupling FNPT with OpenFOAM for Modelling Wave-Structure Interactions with Action of Current," *Ocean Syst Eng*, 8(4), 381–407.
<https://doi.org/10.12989/ose.2018.8.4.381>.

Ransley, E, et al. (2019). "A Blind Comparative Study of Focused Wave Interactions with a Fixed FPSO-like Structure (CCP-WSI Blind Test Series 1)," *Int J Offshore Polar Eng*, ISOPE, 29(2), 113–127. <https://doi.org/10.17736/ijope.2019.jc748>.

Sarpkaya, T, and Storm, M (1985). "In-line Force on a Cylinder Translating in Oscillatory Flow," *Appl Ocean Res*, 7(4), 188–196. [https://doi.org/10.1016/0141-1187\(85\)90025-2](https://doi.org/10.1016/0141-1187(85)90025-2).

Shafieefar, M, and Massie, WW (2001). "In-line Force from Combined Wave and Current Flow on Oscillating Cylinders," *Int J Offshore Polar Eng*, ISOPE, 11(2), 93–98.

Shen, Z, and Wan, DC (2016). "An Irregular Wave Generating Approach Based on Naoe-FOAM-SJTU Solver," *China Ocean Eng*, 30, 177–192. <https://doi.org/10.1007/s13344-016-0010-1>.

Sriram, V, Agarwal, S, and Schlurmann, T (2021). "Laboratory Study on Steep Wave Interactions with Fixed and Moving Cylinder," *Int J Offshore Polar Eng*, ISOPE, 31(1), 19–26. <https://doi.org/10.17736/ijope.2021.jc808>.

Sriram, V, Agarwal, S, Yan, S, et al. (2021). "A Comparative Study on the Nonlinear Interaction Between a Focusing Wave and Cylinder Using State-of-the-art Solvers: Part A," *Int J Offshore Polar Eng*, ISOPE, 31(1), 1–10.
<https://doi.org/10/17736/ijope.2021.jc820>.

Stagonas, D, Buldakov, E, and Simons, R (2018). "Experimental Generation of Focusing Wave Groups on Following and Adverse-Sheared Currents in a Wave-Current Flume," *J Hydraul Eng*, 144(5), 04018016.
[https://doi.org/10.1061/\(ASCE\)HY.1943-7900.0001443](https://doi.org/10.1061/(ASCE)HY.1943-7900.0001443).

Teng, CC, and Nath, JH (1985). "Forces on Horizontal Cylinder Towed in Waves," *J Waterw Port Coastal Ocean Eng*, 111(6), 1022–1040.
[https://doi.org/10.1061/\(ASCE\)0733-950X\(1985\)111:6\(1022\)](https://doi.org/10.1061/(ASCE)0733-950X(1985)111:6(1022)).

Vengatesan, V, Varyani, KS, and Barltrop, NDP (2000). "Wave-Current Forces on Rectangular Cylinder at Low KC Numbers," *Int J Offshore Polar Eng*, ISOPE, 10(4), 276–284.

Yan, S, Ma, et al. (2015). "Numerical and Experimental Studies of Moving Cylinder in Uni-directional Focusing Waves," *Proc 25th Int Ocean Polar Eng Conf*, Kona, HI, USA, ISOPE, 3, 711–718.

Yan, S, Wang, J, Wang, J, Ma, Q, and Xie, Z (2020). "CCP-WSI Blind Test using qaleFOAM with an Improved Passive Wave Absorber," *Int J Offshore Polar Eng*, ISOPE, 30(1), 43–52.
<https://doi.org/10.17736/ijope.2020.jc781>.